Chapter 2
Synthetic Aperture Radar

2.1 Radar Remote Sensing with SAR

Radar is an active microwave remote sensing system, first developed during the Second World War with the purpose of evaluating distances between targets (aircrafts, ships, etc.) and the antenna used to send and receive an Electromagnetic (EM) pulse (Woodhouse 2006; Brown 1999). After the war, the technique stopped being exploited exclusively for aircrafts/ships ranging and found interesting applications in remote sensing of the environment as well. Since its introduction in the remote sensing scientific community, radar has experienced a rapid growth, with the proliferation of numerous applications/techniques exploiting different features of the coherent acquisition of microwaves (Woodhouse 2006).

Microwave has some similarity with optical remote sensing since both acquire the electromagnetic wave scattered from objects on the scene (the similarity is even closer with a LIDAR system). However, the main difference is related to the use of a longer wavelength (i.e. lower frequency), which at the same time represents the foremost radar advantage (Richards 2009). A longer wavelength allows the coherent acquisition of the EM field (i.e. acquisition of amplitude and phase). The information associated with the phase can be exploited with techniques like interferometry and polarimetry which cannot be easily obtained with optical systems (here stereoscopy is not considered as on interferometric technique since it does not work with interferometric fringes) (Bamler and Hartl 1998; Cloude 2009; Papathanassiou and Cloude 2001). In general, the EM radiation interacts with objects with similar or bigger dimension than the wavelength (Stratton 1941; Rothwell and Cloud 2001; Cloude 1995; Woodhouse 2006). Consequently, objects that are small (compared with the wavelength) appear rather transparent to the radiation, and the wave is able to penetrate cluster mediums, composed by collections of particles. For instance, clouds are reasonably transparent to microwaves (especially in lower SAR frequencies) providing measurements with almost

A. Marino, *A New Target Detector Based on Geometrical Perturbation Filters for Polarimetric Synthetic Aperture Radar (POL-SAR)*, Springer Theses,
DOI: 10.1007/978-3-642-27163-2_2, © Springer-Verlag Berlin Heidelberg 2012

any weather conditions. The forest canopy is another example of medium penetrability to some extent by the EM wave. This is one of the major advantages of surveying vegetation with radar. Due to the penetration (which can be tens of meters), the radiation collects information about the forest inner layers (Campbel 2007; Woodhouse 2006; Treuhaft and Siqueria 2000; Cloude et al. 2004).

The Synthetic Aperture Radar (SAR) is an ingenuous radar system which can acquire data with very high resolution. In a standard monostatic architecture, the system is composed of a platform (i.e. airborne or satellite) with the same antenna for transmitter and receiver (Franceschetti and Lanari 1999; Curlander and McDonough 1991; Massonnet and Souyris 2008). While the platform passes over the scene, the antenna transmits a series of EM pulses. Once the pulse reaches an object, an electrical current is exited over the object surface and (generally) generates an EM wave scattered back. Part of the radiation backscattered is recollected by the antenna on the platform (Fig. 2.1). Clearly, different arrangements can be considered, such as a bistatic SAR, where two different antennas are utilised for transmitter and receiver and they generally fly on two different platforms (Cherniakov 2008; Willis 2005). In this thesis, the focus is on monostatic sensors, although the proposed detector can be generalised to bistatic systems (as shown in the following chapters).

The platform moves along the *azimuth* direction with the antenna generally focused on a direction orthogonal to the azimuth: *range* (or slant-range). If the direction of observation is along the platform *nadir* (i.e. straight below the platform) the system is defined *boresight*. On the other hand, when the direction is inclined with an angle ϑ from the zenith, it is defined *side-looking* (the angle ϑ is called *look* angle). A side-looking solution is conventionally to be preferred to boresight for the rejection of range ambiguities (as will be shown in the following) (Franceschetti and Lanari 1999).

The acquisition process is achieved by transmitting a radio pulse (i.e. narrowband signal) and receiving the EM wave backscattered by the targets on the scene. In a classical radar system, the time delay from transmission to reception is related to the speed of the propagating wave and the distance from antenna to object:

$$\Delta t = \frac{2r}{c}, \tag{2.1}$$

where r is the distance between sensor and scatterer and c is the speed of light.

In this basic arrangement, the resolution in range depends on the length of the pulse. Two scatterers can be separated if their distance is bigger than half the duration of the pulse, otherwise the two pulses will overlap each other. Hence, if we define with τ the temporal length of the pulse, the resolution will be:

$$\delta_{sr} = \frac{c\tau}{2} = \frac{c}{2W}, \tag{2.2}$$

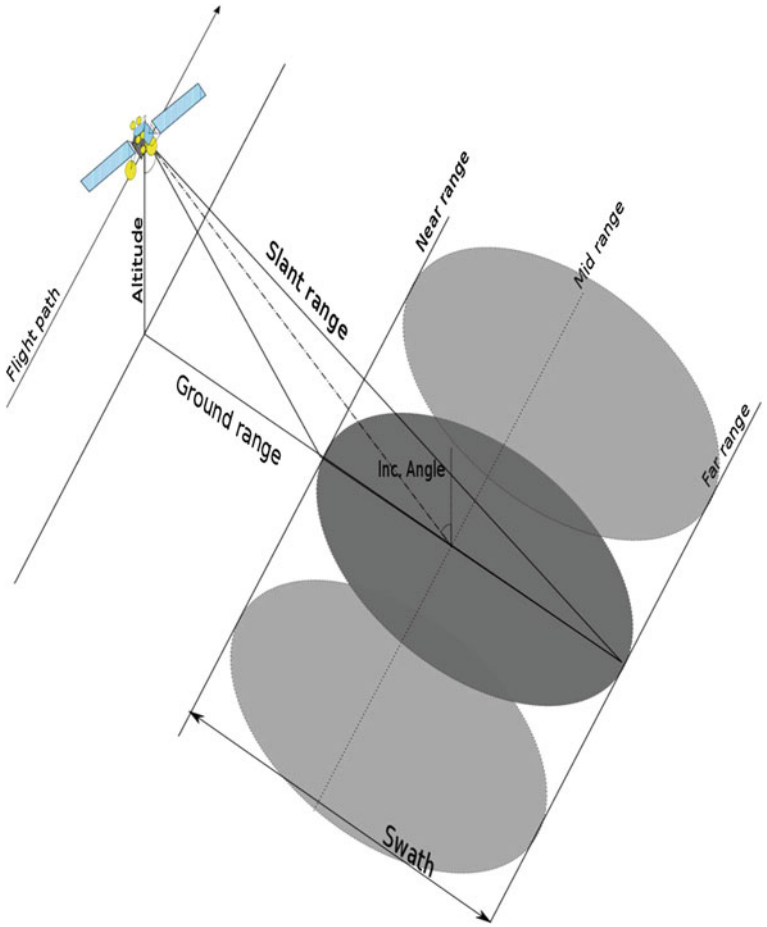

Fig. 2.1 SAR acquisition geometry for a monostatic system (courtesy of Fernando Vicente Guijalba)

where W is the bandwidth of the pulse. Therefore, in order to achieve high resolution the bandwidth must increase, leading to very short effective pulses which are generally not realisable in the designed bandwidth of the system. With the intention of achieving high resolution without decreasing the pulse duration, a frequency modulation was introduced (Curlander and McDonough 1991). The obtained pulse is called a *chirp* and is a linear frequency modulation of the narrowband pulse. It can be written as:

$$f(t) = \cos\left(\omega t + \frac{\alpha t^2}{2}\right) rect\left[\frac{t}{\tau}\right], \tag{2.3}$$

where $\omega = 2\pi f$ is the angular frequency and f is the carrier frequency, *rect* is the rectangular function of duration τ and α is the chirp rate related with the bandwidth W as $\alpha\tau = 2\pi W$. With the chirp, the bandwidth can be increased without reducing the duration of the pulse τ. In order to retrieve the actual scene information, the return must be cleaned from the alteration introduced by the linear phase modulation. This can be accomplished with a match filter with the chirp (and is known as range compression).

Regarding the azimuth resolution, the simplest system is a Real Aperture Radar (RAR). Here, all the points illuminated by the beam-width are collected together, hence they are inseparable. The resolution is dependent on the beam width (or aperture) of the antenna:

$$\Delta x_{RAR} = R\frac{\lambda}{L}, \tag{2.4}$$

where R is the distance between sensor and ground, λ is the wavelength exploited and L is the effective dimension of the antenna. In this configuration, the resolution depends on the distance to the sensor, making satellite applications suited only as scatterometers (Woodhouse 2006). In order to enhance the resolution the dimensions of the antenna or the frequency must increase. However, the frequency is fixed and the antenna cannot be excessively big for structural engineering reasons. A different solution had to be introduced.

The basic idea of the Synthetic Aperture Radar (SAR) is that a point on the ground is illuminated by the antenna not just with one single pulse but with a sequence of pulses. If all the acquisitions for the same point are collected, it will be similar to having performed a single acquisition with an antenna array with length (i.e. aperture) equal to the footprint X. After data compression the azimuth resolution becomes

$$\Delta x_{SAR} = \frac{L}{2}, \tag{2.5}$$

where L is the length of the antenna. Conversely to Eq. 2.4, the resolution improves when the effective dimension of the antenna L is reduced. This seems to contradict common sense since a smaller antenna has a larger beam width (hence a larger footprint). In actual fact, when L decreases, X increases and with it the synthetic antenna. As a consequence the array is larger and the final beam-width is sharper.

After the compression of the row data, the SAR image presents a map of the reflectivity (as a complex value) of the scene, where every pixel represents the coherent sum of the returns from the scatterers located in the resolution cell (Oliver and Quegan 1998). The reflectivity can be expressed with $\rho(r, x)$, where r and x are respectively the range and azimuth of the resolution cells. In any given pixel we have

$$\rho(r, x) = \sum_n \rho_n \delta(r - r_n, x - x_n), \tag{2.6}$$

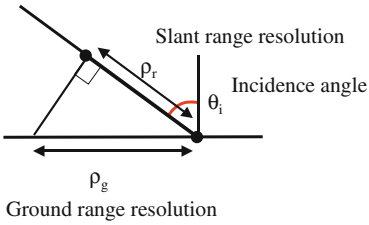

Fig. 2.2 Estimation of ground range resolution (courtesy of Iain Woodhouse)

where δ is the Dirac function and r_n and x_n can move in the resolution cell considered. Therefore, the signal after the processing can be interpreted as a two dimensional complex signal (Massonnet and Souyris 2008).

2.2 Geometrical Distortions

A noteworthy divergence between (active) radar and (passive) optical systems is related to the acquisition arrangement. Radar was first designed with the purpose of acquiring distances between the sensor and the targets on the scene. This attribute is still central in the SAR acquisition strategy. The objects on the scene are arranged depending on the distances from the sensor rather than the location on the ground. Additionally, a radar system needs to be side-looking, where optical systems are often close to nadir. Due to this peculiar acquisition arrangement distortions are introduced on the reflectivity image and the latter cannot be compared straightforwardly with a map or photograph (Woodhouse 2006; Franceschetti and Lanari 1999; Campbel 2007).

Radar measures distances between sensor and scene, therefore distances on the ground (i.e. the horizontal plane where the scene lies) are not preserved and in *near-range* (region closer to the platform) the range resolution is larger than in *far-range* (region further from the platform). A new parameter can be introduced, regarded as *ground-range*, representing the distance measured along the projection of the range (now called *slant-range*) on the horizontal plane. Specifically, the ground range resolution can be calculated as

$$\Delta r_g = \frac{\Delta r}{\sin \vartheta_i}, \tag{2.7}$$

where ϑ_i is the local look angle. Figure 2.2 illustrates the concept of ground range resolution.

Equation 2.7 states that a boresight system (i.e. $\vartheta = 0$) has resolution equal to ∞, since in the hypothesis of plane wave any plane parallel to the ground surface lie only in one single resolution cell. Clearly, the plane wave hypothesis is unsuited in this case and a spherical wave must replace it. The final effect of the variability in ground range resolution is a non linear stretch along the range direction (the near range is compressed).

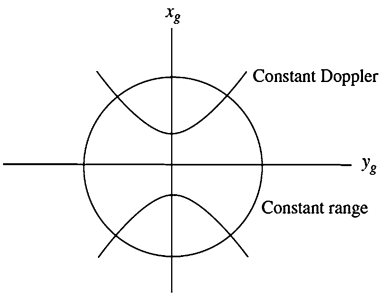

Fig. 2.3 Constant range and constant Doppler curves. The sensor moves along the x_g axis (Mott 2007), as projected onto the ground surface

Equation 2.7 states the importance of side-looking architecture for image formation. Figure 2.3 shows the lines for equi-range and equi-Doppler (Mott 2007). The only way to avoid ambiguities between the two points above and below the y_g axis is simply to focus the antenna only on one side. Although indispensable for image formation, side looking is the cause of distortions in a SAR image.

Figure 2.4 presents the main distortions suffered by a radar image due to the side-looking architecture. The distortions are (Franceschetti and Lanari 1999):

a. Foreshortening: when a slope faces the sensor the illuminated area is compressed in less resolution cells. In other words a larger amount of ground lies in the same resolution cell since the apparent local look angle (calculated with the normal of the surface) is reduced. In a SAR image foreshortening produces a shift of the side of mountains (or generally slopes) facing the sensor in the direction of the sensor. Moreover, it is generally accompanied by a rising in backscattering since the number of scatterers in the same resolution cell increases (the energy of all the scatterers is compacted in a smaller area).
b. Layover: when the steepness of the slope facing the sensor is higher than the look angle the return from the top of the object comes before the one from the bottom. If compared with an optical image, the layover flips top and bottom. Layover is rather common in SAR imaging, since it affects all the vertical structures with changes in height bigger than the resolution cell (i.e. buildings, trees).
c. Shadowing: this effect is observable on the slopes opposite to the sensor and it can be interpreted as the opposite of foreshortening. The areas affected by shadowing are enlarged (along the range direction). When the slope is smaller than $\vartheta - \pi/2$, the areas become completely dark (in optical shadow).

In general, shadowing areas (i.e. slopes facing away from the sensor) are darker since the energy is spread over a larger area or they are not visible at all (additionally the surfaces scatter less as predicted by the Bragg model).

Another cause of distortion in a SAR image is associated with the dissimilar resolutions in range and azimuth. In the image formation, the range resolution depends on the bandwidth (Eq. 2.2) while the azimuth one depends on the length of the antenna (Eq. 2.5). As a result, the pixel will not generally be square but rather rectangular on the ground. A rectangular pixel stretches the image in the

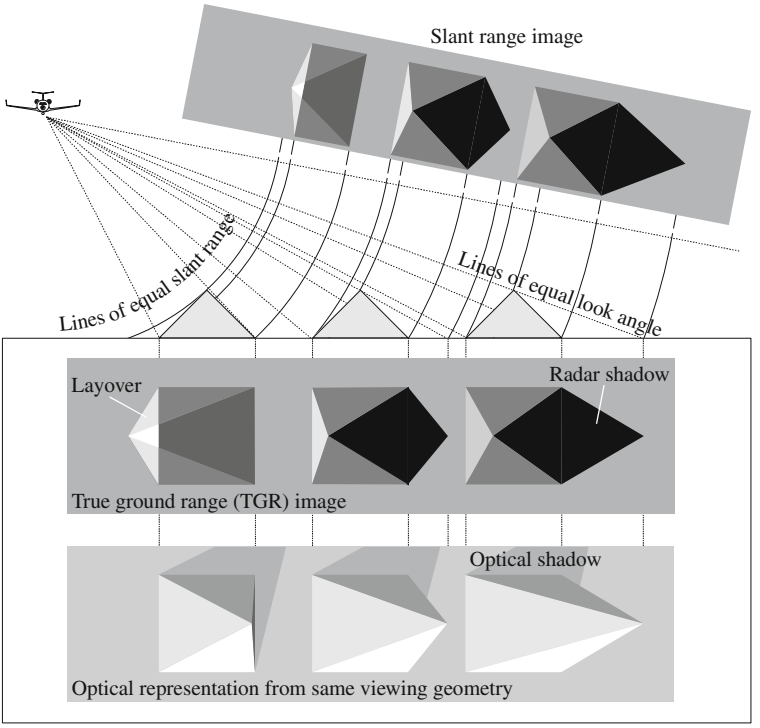

Fig. 2.4 Distortions suffered by the side looking architecture compared with a optical viewing geometry (courtesy of Iain Woodhouse)

direction where the resolution is higher (for satellite applications often this is the azimuth).

Due to the severe distortions affecting a SAR image, the latter cannot be overlapped straightforwardly with a map. As a first step, the image must be geo-coded in order to correct the geometric distortions. Subsequently, it must be projected on a coordinate system with a geo-location. In the validation of the proposed detector, in the current work, geo-location of the images is not performed since the detector works with the physics of the backscattering (polarimetry) and this does not change with geo-location (as long as the geo-location is well defined) (Campbel 2007; Wise 2002).

2.3 Statistical Characterisation of Targets

The backscattered field acquired by a SAR system is a product of the interaction between objects on the scene and the microwave pulse sent by the transmitter

antenna. The interaction is generally more consistent when the dimensions of the illuminated object are equal or bigger than the wavelength (Stratton 1941; Rothwell and Cloud 2001). In microwave remote sensing, the wavelength is around centimetres (X- or C-band) or tens of centimetres (S-, L- and P-band) while the resolution cell is around meters. For this reason, in the same resolution cell several scatterers contribute to the total backscattered field. For the theorem of superimposition of fields, all the EM waves coming from the same resolution cell are summed coherently together (generally the phases must be taken into account and the total power is not the sum of the power contributions) (Oliver and Quegan 1998; Rothwell and Cloud 2001).

If the return from the *ith* scatterer in the cell is $V_i e^{j\phi_i}$ the total return will be:

$$V_{re} + jV_{im} = V = \sum_{i=1}^{N} V_i e^{j\phi_i} = \sum_{i=1}^{N} V_i \cos\phi_i + j\sum_{i=1}^{N} V_i \sin\phi_i. \tag{2.8}$$

The possibility to represent the EM wave with a complex number will be illustrated in the next section. Equation 2.8 describes the coherent sum of the contributions in the cell. If there is not a single dominant scatterer, the only way to extract information about the observed scatterers is to treat the problem with a statistical approach (Oliver and Quegan 1998). In fact, the number of observables (i.e. real and imaginary part of the total return) is smaller than the number of unknowns.

If N is big enough, we can apply the central limit theorem and say that the real and imaginary part of the return are normally distributed: $V_{re} \sim N(0, \sigma^2)$ and $V_{im} \sim N(0, \sigma^2)$. Their probability density functions (*pdf*) are

$$\begin{aligned} f_{V_{re}}(V_{re}) &= \frac{1}{\sqrt{2\pi\sigma^2}} \exp\left(-\frac{V_{re}^2}{2\sigma^2}\right), \\ f_{V_{im}}(V_{im}) &= \frac{1}{\sqrt{2\pi\sigma^2}} \exp\left(-\frac{V_{im}^2}{2\sigma^2}\right). \end{aligned} \tag{2.9}$$

The mean is zero, $E[V_{re}] = E[V_{im}] = 0$, since the average of random real numbers with their sign is zero (Gray and Davisson 2004; Kay 1998; Papoulis 1965).

Furthermore, the real and imaginary parts are independent of each other which makes them uncorrelated:

$$E[V_{re}V_{im}] = E[V_{re}]E[V_{im}] = 0, \tag{2.10}$$

where $E[.]$ stands for *expected value*.

The trend of a Gaussian random variable with zero mean and variable standard deviation σ is plotted in Fig. 2.5.

The SAR image displays the reflectivity of a scene and it can be represented as a matrix of complex numbers. The amplitude of such complex numbers keeps valuable information about the amount of backscattering coming from the

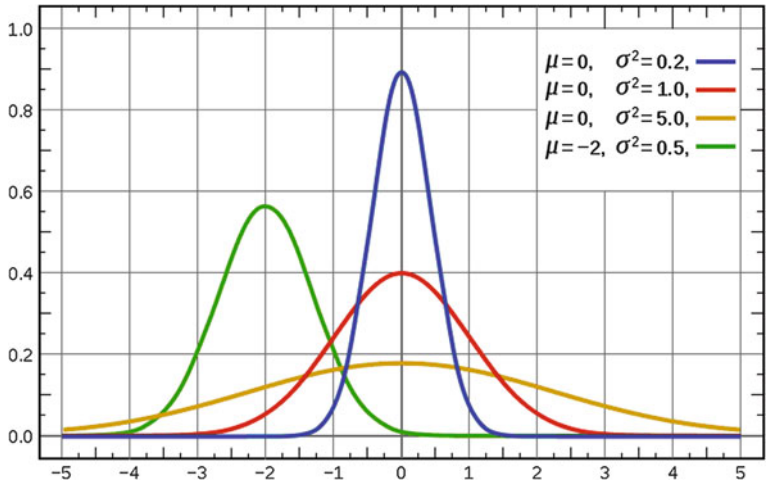

Fig. 2.5 Gaussian distribution with variable mean and standard deviation

resolution cell (since it is the square root of the power). Using the *pdf* of real and imaginary parts, it is possible to extract the joint *pdf* of amplitude and phase of the backscattering

$$f_{V\phi}(V,\phi) = \frac{V}{\sqrt{2\pi\sigma^2}}\exp\left(-\frac{V^2}{2\sigma^2}\right). \tag{2.11}$$

Integrating the expression in Eq. 2.11 on the entire interval of the phase, the *pdf* of the amplitude can be extracted

$$f_V(V) = \int_0^{2\pi} f_{V\phi}(V,\phi)d\phi = \frac{V}{\sigma^2}\exp\left(-\frac{V^2}{2\sigma^2}\right),\ V \geq 0 \tag{2.12}$$

The latter corresponds to a Rayleigh distribution defined in $[0,\infty]$ and regarded as $V \sim Rayleigh(\sigma)$ (Papoulis 1965).

A quick way to characterise a random variable is using its principal modes. They can be obtained by integrating the expression of the *pdf* as shown in the following:

$$E[V] = \int_0^{\infty} V f_V(V)dV = \sqrt{\frac{\pi}{2}}\sigma, \tag{2.13}$$

$$E\left[V^2\right] = \int_0^{\infty} V^2 f_V(V)dV = 2\sigma^2, \tag{2.14}$$

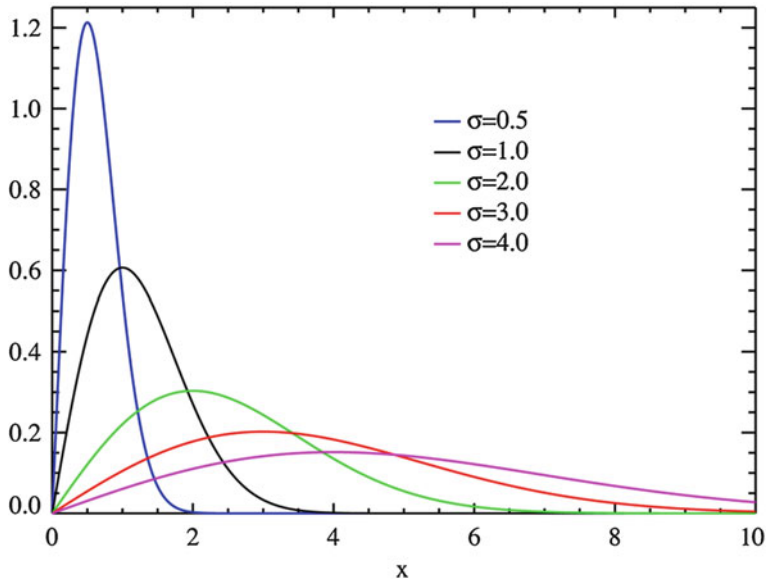

Fig. 2.6 Rayleigh distribution for variable σ

$$VAR[V] = E\left[V^2\right] - E[V]^2 = \frac{4-\pi}{2}\sigma^2. \tag{2.15}$$

Figure 2.6 shows the Rayleigh distribution. As expected the probability of negative values is zero and the variation becomes bigger when the mean increases.

The *pdf* of the phase can be extracted as well and is uniformly distributed in $[0, 2\pi]$.

Once the statistical distribution of the amplitude is obtained, we can describe the power distribution of the backscattering, i.e. $W = V^2$. After some manipulation the *pdf* of the power is found as

$$f_W(W) = \frac{1}{2\sigma^2}\exp\left(-\frac{W}{2\sigma^2}\right),\ W \geq 0. \tag{2.16}$$

which coincides with an exponential random variable. The latter is generally indicated with $W \sim Exp(\lambda)$, where λ is linked to the mean. The modes can be estimated:

$$E[W] = 2\sigma^2 = 1/\lambda, \tag{2.17}$$

$$E\left[W^2\right] = 8\sigma^4, \tag{2.18}$$

$$VAR[W] = E\left[W^2\right] - E[W]^2 = 4\sigma^4. \tag{2.19}$$

The mean of the exponential is ordinarily indicated with $1/\lambda$.

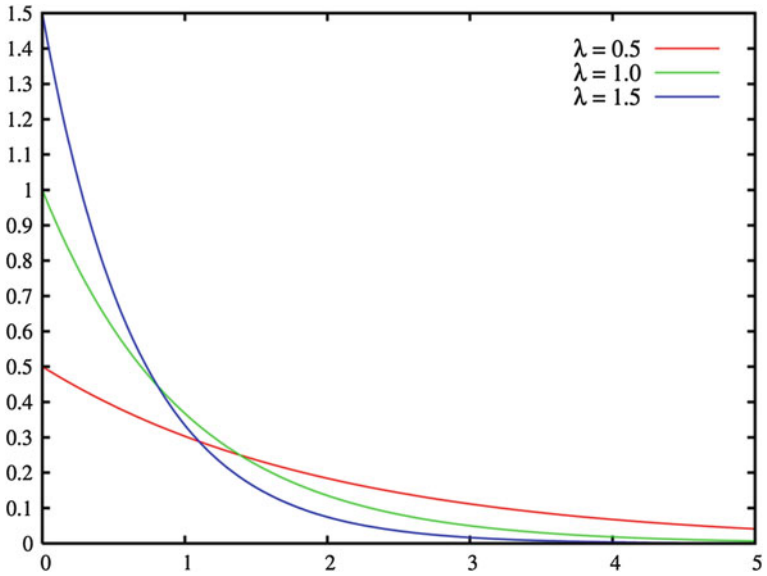

Fig. 2.7 Exponential distribution for variable λ

Figure 2.7 presents the Exponential distribution when the mean is varied. As in the case of a Rayleigh distribution, the variability of the Exponential is large and the standard deviation increases linearly with the mean (they are actually the same). This huge variation can lead to significant estimation errors making the scattering description on the basis of a single pixel a challenge.

In general, to reduce the variability of random variables, the average of independent and identically distributed (*iid*) realisations can be considered (please note, not all random variables when averaged reduce their variability).

If $W_1, \ldots, W_N$ are Exponential distributions, then the variable $\gamma = \sum_{i=1}^{N} W_i$ is a Gamma distribution indicated as $\gamma \sim \Gamma(\vartheta, k)$ where k is the *shape* factor depending on the number of elements summed (i.e. $k = N$) while $\vartheta = 1/\lambda = 2\sigma^2$ is the *scale* factor depending on the mean of the Exponential variables. The *pdf* is equal to:

$$f_{\overline{W}}(\overline{W}) = \left(\frac{N}{2\sigma^2}\right)^N \frac{\overline{W}^{N-1}}{(N-1)!} \exp\left(-\frac{N\overline{W}}{2\sigma^2}\right). \tag{2.20}$$

And its modes are:

$$E\left[\overline{W}\right] = 2N\sigma^2, \tag{2.21}$$

$$VAR\left[\overline{W}\right] = 4\sigma^4. \tag{2.22}$$

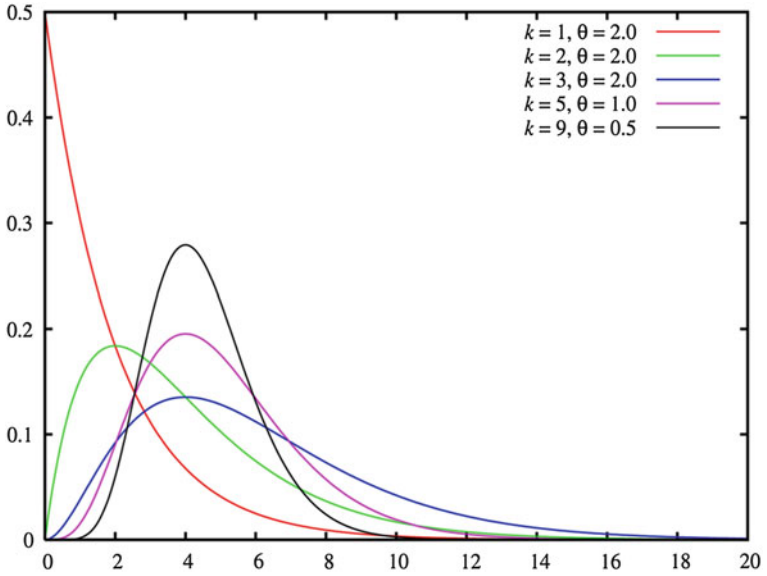

Fig. 2.8 Gamma distribution for variable k and ϑ

Commonly, the sum of Exponential is subsequently normalised by the number of samples N in order to achieve the average $\overline{W} = \frac{1}{N}\sum_{i=1}^{N} W_i$. The resulting random variable will be a scaled Γ distribution, $\overline{W} \sim \Gamma\left(\frac{\vartheta}{N}, k\right)$, and the modes will be:

$$E[\overline{W}] = 2\sigma^2, \tag{2.23}$$

$$VAR[\overline{W}] = \frac{4\sigma^4}{N}, \tag{2.24}$$

Figure 2.8 illustrates the Γ distribution with variable shape and scale factors.

The variance of the random variable is reduced by increasing the number of independent samples averaged. In order to obtain the desired reduction of variability, the sum must be performed on independent samples with the same mean (independent and identically distributed, *iid*). There are several methodologies to select independent samples in a SAR image. The most common (and the one used in this thesis) considers the average over neighbouring pixels with a moving window, but, more complicated strategies can be exploited.

2.4 Radar Cross Section

The aim of microwave remote sensing is extracting information from the EM wave scattered by an object. In particular, the power of the backscattering was the

Table 2.1 RCS for standard shapes (Franceschetti and Lanari 1999)

Shape	Sphere radius d	Square plate: side d	Triangular trihedral: side d	Square trihedral: side d
RCS [m^2]	πd^2	$4\pi\frac{d^4}{\lambda^2}$	$\frac{4\pi}{3}\frac{d^4}{\lambda^2}$	$12\pi\frac{d^4}{\lambda^2}$

subject of extensive studies when phase measurements where not yet feasible. A parameter called *radar cross section* (*RCS*) $\sigma[m^2]$ was introduced and it represents the area of an equivalent sphere (assumed as a perfect reflector) scattering the same amount of power as the target (Franceschetti and Lanari 1999; Woodhouse 2006). In a complex object, the power backscattered also depends on the angle of view of the target. Additionally, the induced currents on the surface of the object radiate in many directions and a directivity pattern of the object can be estimated.

If polar coordinates are introduced, the directions of incident and scattered wave can be characterised by the pairs (ϑ_i, φ_i) and (ϑ_s, φ_s) respectively. In conclusion, the *RCS* can be described as function of the direction for incident and scattered wave. Integrating over all the directions of the scattered wave (for a fixed incident wave), the total scattered power can be calculated as (Woodhouse 2006)

$$S(r, \vartheta_s, \varphi_s) = \frac{S_i(\vartheta_i, \varphi_i)\sigma(\vartheta_i, \varphi_i; \vartheta_s, \varphi_s)}{4\pi r^2}. \tag{2.25}$$

where r is the distance.

In the case of backscattering, the direction of incident and scattered waves is the same. Hence, $\vartheta_i = \vartheta_s$ and $\varphi_i = \varphi_s$.

For some simple shapes the calculation of the *RCS* is possible analytically (after various approximations). Some of these targets are considered in Table 2.1.

The *RCS* increases relatively fast in the case of corners (with the fourth power of the side), since they are able to collect the power of the illuminating wave in a narrow beam. The dependence on λ is related to the increased apparent dimensions of the surfaces.

The expression of the density of power can be used to estimate the power received by the system from an object at distance r:

$$P_r = \frac{PGA\sigma}{(4\pi)^2 r^4} = \frac{PG^2\lambda^2\sigma}{(4\pi)^3 r^4} = \frac{PA^2\sigma}{4\pi\lambda^2 r^4}. \tag{2.26}$$

where P is the peak power transmitted, G is the antenna gain and A is the antenna effective area.

It is interesting to note that the power goes down with the fourth power of the distance, which is because far from the source it propagates as a spherical wave with a dispersion of intensity as the square of the distance. Subsequently, the two way attenuation must be taken into account (by multiplying the two attenuations). The estimation of the theoretical power received is relevant in SAR image

formation since a different power compensation for near and far range must be performed in order to have a reliable map of the scene reflectivity (Herwig 1992).

2.5 Polarimetric Acquisition: The Scattering Matrix

In this section the principles of radar polarimetric acquisition are introduced, specifically the formation of the scattering matrix, while a more complete treatment will be provided in the next chapter.

2.5.1 The Scattering Matrix

For the sake of brevity, the treatment will start from the definition of narrowband signals, leaving out the electromagnetism theory that deals with the derivation of the wave equations. If the bandwidth of the signal is small compared with the carrier frequency, the latter can be ignored and the electric (or magnetic) field can be represented with complex scalars. In the monochromatic case, the problem can be rigorously treated with fasors (Rothwell and Cloud 2001). Far from the source, the propagation is accomplished with a spherical wave that can be locally approximated as plane wave. The wave front is a plane and the electric and magnetic fields are orthogonal to the direction of propagation. Such propagation is equivalently regarded as Transverse ElectroMagnetic (*TEM*) since the fields lie in the transverse plane (Stratton 1941).

Figure 2.9 shows the coordinate system exploited.

The electric field can be written as

$$\underline{E} = E_x \underline{u}_x + E_y \underline{u}_y, \tag{2.27}$$

where the propagation is accomplished in the z direction and E_x, E_y, are complex numbers.

Hence, it can be written:

$$E_x = |E_x| e^{j\phi_x} \text{ and } E_y = |E_y| e^{j\phi_y}. \tag{2.28}$$

While the wave moves in space/time, the phase of the electric field changes. This effect can be taken into account with

$$E_x = |E_x| e^{j(\omega t - kz + \phi_x)} \text{ and } E_y = |E_y| e^{j(\omega t - kz + \phi_y)}. \tag{2.29}$$

where ω is the angular frequency $\omega = 2\pi f$, t is the time and k is the wavenumber $k = \frac{\omega}{c}$, with c speed of light in the medium considered. ϕ_x *and* ϕ_y give an initial phase for the two components.

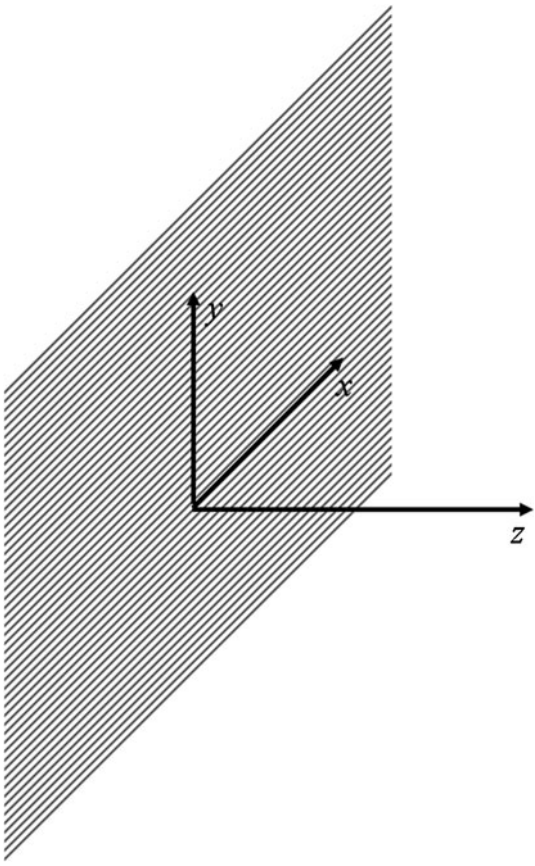

Fig. 2.9 Coordinate system in agreement with the propagating wave (z direction)

Once the information about the frequency is reintroduced in Eq. 2.27, the expression can be reconverted in time domain (real numbers) with:

$$e_x = \mathrm{Re}\left\{|E_x|e^{j(\omega t - kz + \phi_x)}\right\} = |E_x|\cos(\omega t - kz + \phi_x),$$
$$e_y = \mathrm{Re}\left\{|E_y|e^{j\left(\omega t - kz + \phi_y\right)}\right\} = |E_y|\cos\left(\omega t - kz + \phi_y\right). \tag{2.30}$$

The two components of the field (i.e. x and y) interact coherently with each other producing a resulting vector that moves on the plane of propagation. The polarisation of the EM field is related to the shape that the electric field draws on the transverse plane while the time passes. In this brief introduction, only stationary states of polarisation are considered. Specifically, if the electric field has a component only in one axis of the propagation plane its polarisation is defined to be linear (in general in order to have linear polarisations the two components must have the same phase).

When a target is excited by a wave which is linearly polarised in the x direction, $\underline{E}^i = E_x^i \underline{u}_x$, the scattered wave will be (Krogager 1993; Kennaugh and Sloan 1952; Mott 2007; Cloude 2009; Lee and Pottier 2009)

$$\underline{E}^s = E_x^s \underline{u}_x + E_y^s \underline{u}_y = \frac{1}{\sqrt{4\pi r^2}} \left[S_{11} E_x^i \underline{u}_x + S_{21} E_x^i \underline{u}_y \right]. \tag{2.31}$$

since the reradiated wave has generally a different polarisation from the incident one (as will be explained in the next section). Consequently, for any incident wave at least two measurements are necessary to characterise the scattered field (i.e. the x and y components).

The final requirement is to be able to describe the target scattering behaviour independently of the incident wave employed. Thus, the x component of the incident field alone is not sufficient since it is not sufficient to describe all the possible incident waves. The orthogonal component y must be considered as well. Therefore, a linear polarised field in the y direction can be transmitted and the return collected in the two components:

$$\underline{E}^s = E_x^s \underline{u}_x + E_y^s \underline{u}_y = \frac{1}{\sqrt{4\pi r^2}} \left[S_{12} E_y^i \underline{u}_x + S_{22} E_y^i \underline{u}_y \right]. \tag{2.32}$$

In summary, in order to describe completely the polarimetric behaviour of a target four acquisitions are needed: two to describe any scattered wave multiplied by two to describe any incident wave. The theorem of superposition of fields asserts that the four measurements can be done separately (but the target must not change). The four measurements can be collected in a matrix as

$$\underline{E}^s = \begin{bmatrix} E_x^s \\ E_y^s \end{bmatrix} = \begin{bmatrix} S_{11} & S_{12} \\ S_{21} & S_{22} \end{bmatrix} \begin{bmatrix} E_x^i \\ E_y^i \end{bmatrix} \frac{1}{\sqrt{2\pi r^2}}. \tag{2.33}$$

The matrix

$$[S] = \begin{bmatrix} S_{11} & S_{12} \\ S_{21} & S_{22} \end{bmatrix} \tag{2.34}$$

is called the *scattering* (or *Sinclair*) matrix. With the scattering matrix any stationary target illuminated by a wave with stationary polarisation can be completely characterised (Kennaugh and Sloan 1952). The hypothesis of stationarity seems to be unavoidable; however in the next section we will see that in the case of non-stationary processes we can still characterise a target exploiting its statistics.

When the scattering matrix is completely acquired in one single flight pass of the platform, the system is defined as *quad* polarimetric. The simultaneous acquisition is needed to reconstruct properly the polarimetric characteristic of the target, especially if this changes from one acquisition to another. However, in some cases, the sensor is not sufficiently complex to acquire $[S]$ in one pass, but only half (for instance one column of the scattering matrix). In this scenario, the

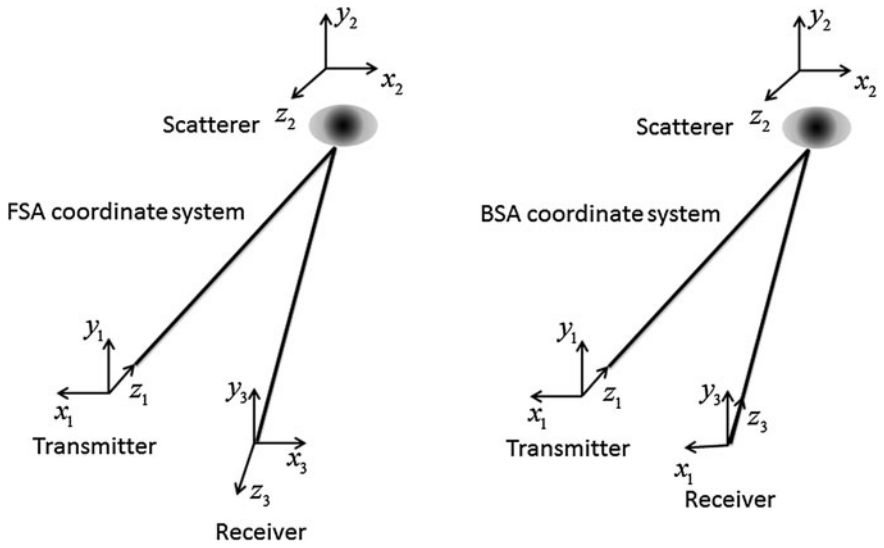

Fig. 2.10 Comparison of FSA and BSA coordinate systems

system is defined as *dual* polarimetric. Unfortunately, the latter is not able to describe completely a polarimetric target (Cloude 2009; Lee and Pottier 2009).

2.5.2 The Coordinate System

The correct selection of the coordinate system for a scattering problem is often a key point, since an advantageous selection can reveal symmetries which simplify drastically the treatment of the problem (Cloude 1995).

The most common choice is to set the coordinate system in agreement with the propagating wave (on the plane wave). This strategy takes the name of *Forward (anti-monostatic) Scattering Alignment (FSA),* and it is probably the optimum alternative when the scattering occurs in any direction (as in the bistatic case). However, in general, the transmitter and receiver antennas are the same (i.e. monostatic system). In this situation, a coordinate system in agreement with the antenna can be employed since the antenna remains fixed. Such a coordinate system is regarded as *Back (Bistatic) Scattering Alignment (BSA).* Figure 2.10 shows the comparison of the two arrangements (Boerner 2004).

The targets observed in a radar image are commonly reciprocal in the microwave range of frequencies. In the case of a monostatic arrangement and reciprocal medium the scattering matrix becomes symmetric since for the reciprocal theorem for antennas the same antenna behaves equally in transmission and reception (i.e. the scatterer can be interpreted as an antenna itself). Therefore, the two off-diagonal terms of [*S*] are the same. Please note, with the *FSA* arrangement the

symmetry of [*S*] cannot be exploited. This symmetry introduces a significant simplification in the problem since only 3 complex numbers rather than 4 are necessary to characterise the target (Cloude 1995). Additionally, a symmetric matrix can be diagonalised with (generally) complex eigenvalues. The eigenvectors represent the optimum polarisations for the scattering problem, as will be presented in the next chapter (Huynen 1970; Kennaugh and Sloan 1952).

In this thesis, when it is not indicated otherwise, the *BSA* arrangement will be used, since it has been shown to be more advantageous for the study of backscattering problems.

References

Bamler R, Hartl P (1998) Synthetic aperture radar interferometry. Inverse Probl 14:1–54
Boerner WM (2004) Basics of radar polarimetry. RTO SET Lecture Series
Brown L (1999) A radar history of world war II, technical and military imperatives. Institute of Physics Publishing, Bristol and Philadelphia
Campbel JB (2007) Introduction to remote sensing. The Guilford Press, New York
Cherniakov M (2008) Bistatic radar: emerging technology. Wiley, Chichester
Cloude RS (1995) An introduction to wave propagation & antennas. UCL Press, London
Cloude SR (1995) Lie groups in EM wave propagation and scattering. Chapter 2 in electromagnetic symmetry. In: Baum C, Kritikos HN (eds). Taylor and Francis, Washington, ISBN 1-56032-321-3, pp 91–142
Cloude SR (2009) Polarisation: applications in remote sensing. Oxford University Press, Oxford, 978-0-19-956973-1
Cloude SR, Corr DG, Williams ML (2004) Target detection beneath foliage using polarimetric synthetic aperture radar interferometry. Waves Random Complex Media 14:393–414
Curlander JC, Mcdonough RN (1991) Synthetic aperture radar: systems and signal processing. Wiley, New York
Franceschetti G, Lanari R (1999) Synthetic aperture radar processing. CRC Press, Boca Raton
Gray RM, Davisson LD (2004) An introduction on statistical signal processing. Cambridge University Press, Cambridge
Herwig O (1992) Radiometric calibration of SAR systems. In: fundamentals and special problems of synthetic aperture radar (SAR), AGARD Lecture Series, Vol 182
Huynen JR (1970) Phenomenological theory of radar targets. Delft Technical University, The Netherlands
Kay SM (1998) Fundamentals of statistical signal processing, vol 2: Detection theory. Prentice Hall, Upper Saddle River
Kennaugh EM, Sloan RW (1952) Effects of type of polarization on echo characteristics. Ohio state University, Research Foundation Columbus, Quarterly progress reports (In lab)
Krogager E (1993) Aspects of polarimetric radar imaging. Technical University of Denmark, Lyngby
Lee JS, Pottier E (2009) Polarimetric radar imaging: from basics to applications. CRC Press, Boca Raton
Massonnet D, Souyris JC (2008) Imaging with synthetic aperture radar. EPFL Press, CRC Press, Boca Roton
Mott H (2007) Remote sensing with polarimetric radar. Wiley, Hoboken
Oliver C, Quegan S (1998) Understanding synthetic aperture radar images. Sci Tech Publishing, Inc., Raleigh

Papathanassiou KP, Cloude SR (2001) Single-baseline polarimetric SAR interferometry. IEEE Trans Geosci Remote Sens 39:2352–2363
Papoulis A (1965) Probability, random variables and stochastic processes. McGraw Hill, New York
Richards, JA (2009) Remote sensing with imaging radar—signals and communication technology. Springer-Verlag Berlin and Heidelberg GmbH & Co. KG, Germany
Rothwell EJ, Cloud MJ (2001) Electromagnetics. CRC Press, Boca Raton
Stratton JA (1941) Electromagnetic theory. McGraw-Hill, New York
Treuhaft RN, Siqueria P (2000) Vertical structure of vegetated land surfaces from interferometric and polarimetric radar. Radio Sci 35:141–177
Willis NJ (2005) Bistatic Radar. SciTech, Releigh
Wise S (2002) GIS basics. Taylor & Francis, London
Woodhouse IH (2006) Introduction to microwave remote sensing. CRC Press, Taylor & Francis Group, Boca Raton

http://www.springer.com/978-3-642-27162-5

A New Target Detector Based on Geometrical Perturbation Filters for Polarimetric Synthetic Aperture Radar (POL-SAR)

Marino, A.

2012, XXII, 242 p., Hardcover
ISBN: 978-3-642-27162-5